Presented at the 22nd European Photovoltaic Solar Energy Conference and Exhibition, 3 - 7 September 2007, Milan, Italy.

ADVANCES IN INFRARED IMAGING METHODS FOR SILICON MATERIAL CHARACTERIZATION

Martin C. Schubert[1], Manuel The[2], Paul Gundel[2], Martin Kasemann[1], Sebastian Pingel[2], Wilhelm Warta[2]
[1] Freiburger Materialforschungszentrum, University of Freiburg, Stefan-Meier-Str. 21, 79104 Freiburg, Germany
[2] Fraunhofer Institute for Solar Energy Systems (ISE), Heidenhofstr. 2, 79110 Freiburg, Germany

ABSTRACT: Infrared imaging methods have been demonstrated as being valuable means to extract information about material quality. The main parameters under investigation are the minority carrier lifetime, the free carrier density (base doping, emitter diffusion), and the trap density. Infrared imaging methods are mainly based on the detection of infrared radiation emitted by the sample. Depending on the origin of the radiation, recombination luminescence in the near infrared or free carrier emission in the mid wavelength infrared is recorded. We present the state of the art of infrared imaging techniques for silicon material. These include Carrier Density Imaging / Infrared Lifetime Mapping, Photoluminescence Imaging for fast lifetime measurements, and trap density measurements for advanced defect characterization. Emphasis is put on the correction of spurious surface effects, on calibration techniques for Photoluminescence Imaging, on progress in trap characterization, and on diffusion length measurements on solar cells.
Keywords: Experimental methods, Infrared Imaging, free carrier density

1 CONCEPT OF INFRARED IMAGING

Various infrared imaging techniques for material characterization in the field of silicon photovoltaics have been developed in the recent years [1-6]. The emission spectrum of silicon provides, among others, information about free carrier density and defects. Since reabsorption processes of the detectable infrared photons are moderate, information about bulk properties can be retrieved. Two main emission processes determine the detectable spectrum: (i) band-to-band recombination causing a broad photoluminescence peak at 1100 nm and (ii) infrared photon emission by free carriers in the mid and long wavelength infrared. If reabsorption is neglected, photoluminescence radiation intensity is proportional to the product of free electron and free hole concentration, whereas free carrier emission is proportional to the sum of both, weighted with the absorption coefficients for electrons and holes, respectively. Trapping [7] and Depletion Region Modulation (DRM) effects [8] do not interfere with the photoluminescence measurement. Under illumination, the free minority carrier density and thus the carrier lifetime can be determined if the base doping is known. Trupke et al. [9] have developed a lifetime calibration method for integral PL measurements which takes transient effects into account. In the dark, no signal can be detected with PL.

In contrast to photoluminescence, free carrier emission can be detected on illuminated and non-illuminated samples. Under dark conditions, the signal is proportional to the doping concentration. Information about base and emitter doping can be obtained. The difference between illuminated and dark state allows to determine the free carrier density and the lifetime. Calibration can be performed with samples of known doping concentration. Trapping can be detected under low-injection. The modeling of the total trap density gives access to a new material parameter.

The measurement techniques presented take advantage of fast data acquisition by infrared cameras. Different cameras are available at ISE to detect photons from the visible to 1100 nm (Si), 3.5 µm to 5 µm (CdHgTe), and 3.7 µm to 5.1 µm (InSb). Free excess carrier generation is homogeneously performed by semiconductor diode lasers with an optical power between 30 W and 120 W and wavelengths of 804 nm and 940 nm.

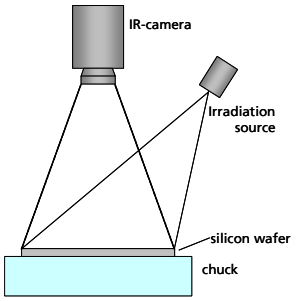

Figure 1: Setup for infrared imaging. Depending on the method, different cameras and irradiation sources are implemented.

Typically, the sample under test is mounted on a thermostated mirror where the camera is focused on (see Fig. 1).

2 DETECTION OF PHOTONS EMITTED THROUGH ROUGH SURFACES

A crucial point is an appropriate consideration of surface conditions. Up to now, restrictive conditions for the surface quality had to be fulfilled for correct quantitative measurements. Measurements on rough surfaces may yield blurred images with increased signal. This is especially pronounced for measurements with detected wavelengths larger than 1000 nm. We present an analytical correction method for Carrier Density Imaging (CDI), also called Infrared Lifetime Mapping (ILM), as example. The emissivity of the sample is determined for that purpose and a deconvolution procedure is established which accounts for spurious blurring effects.

Flat surfaces allow for a sharp image of the photon source distribution, i.e. the carrier density in our case, since only rays with low angle towards the surface normal vector can reach the camera. Rays with larger

angles are refracted or totally reflected and do not reach the camera aperture. In contrast, rough surfaces scatter incident rays. Total internal reflection is decreased and rays with larger angles may be scattered towards the camera. Thus, carrier emissen originating in a specific point in the sample may be detected as emitted from a broadened surface area ("blurring").

The effect of rough surfaces can be observed by comparing two neigbouring wafers from a multicrystalline silicon block with different surface conditions: The reference measurement is performed on a chemically polished sample, whereas the other measurement is done on a sample with an alkaline etched, rough surface. Both, the absolute value and the spatial distribution are affected by the surface roughness (see Fig. 2).

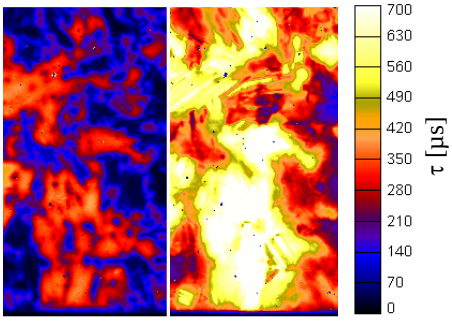

Figure 2: Uncorrected lifetime measurements on a chemically polished sample (left) and an alkaline etched, adjacent sample (right).

The spuriously increased lifetime may be corrected by taking the emissivity of the sample into account. For CDI measurements the emissivity can be easily obtained from an image of the sample taken in the dark. In Fig. 3, the photon flux density of the sample, detected by the camera, is plotted versus the photon flux density of a black surface for various temperatures. The plot shows results for a wafer with chemically polished surfaces, for a wafer with rough, alkaline etched surfaces, and for an as-cut wafer. In all cases the behavior can be approximated as linear. The slope may be interpreted as emissivity. For more details, please refer to [10].

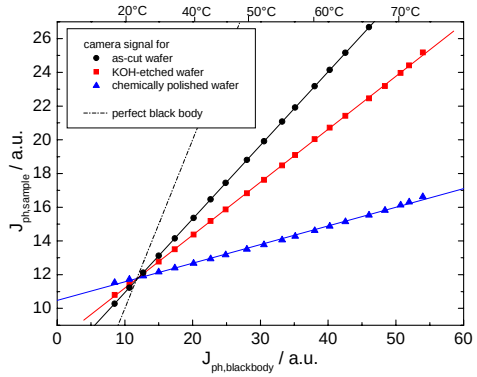

Figure 3: Photon flux density of silicon sample with different surface conditions versus photon flux density of blackbody at the same temperature. Each data point corresponds to a specific wafer temperature.

Since all curves cross at room temperature, it is sufficient to take one single camera image at a specific temperature above ambient temperature to determine the gradient $m_{Jph,rough}$ from Fig. 3 for each camera pixel. Applying the correction

$$\tau_{corr}(x,y) = \frac{m_{Jph,ref}}{m_{Jph,rough}(x,y)} \tau_{rough}(x,y) \qquad (1)$$

yields a corrected measurement shown in Fig. 4. $m_{Jph,ref}$ is the gradient measured on a sample with flat surfaces but same thickness and doping concentration.

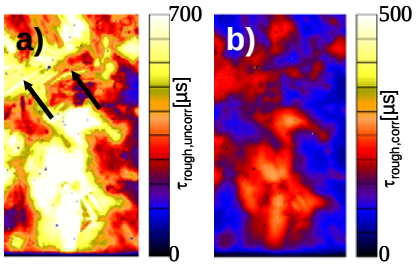

Figure 4: CDI measurement before and after emissivity correction

Although blurring is still present in the corrected measurement, the absolute value is comparable to the reference measurement (see Table I).

Table I: Comparison of mean values

	arithmetic mean value
τ_{ref}	157 µs
$\tau_{rough,uncorrected}$	448 µs
$\tau_{rough,corr}$	143 µs

Artefacts in the CDI measurement induced by distinct surface structures (see arrows in Fig. 4) are well corrected. The remaining blurring effect can be removed by a numerical deconvolution procedure. If PSF(x,y) is the signal of a point source (point spread function), detected with the camera through the rough surface, the signal for an arbitrary lifetime distribution $\tau_{rec}(x,y)$ can be described as a convolution integral:

$$\tau_{rough}(x,y) = \int \tau_{rec}(x-x', y-y')\, PSF(x',y')\, dx'dy' \qquad (2)$$

The point spread function is determined from a CDI measurement with point-focused laser instead of a homogeneous illumination. Fig. 5 shows a linescan of the corresponding CDI signal. Instead of a point-like shape a broadened peak is observed. Empirically, a Lorentz fit has turned out to describe the measured peak with sufficient accuracy.

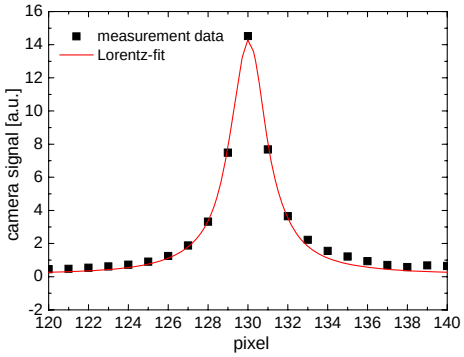

Figure 5: Linescan through CDI measurement with point-focused excitation source. One pixel corresponds to 350 µm.

Solving equation (2) for τ_{rec} can be numerically performed in Fourier space. Instead of the integral a simple multiplication describes the convolution. The concept of Wiener filtering is finally applied to calculate the corrected lifetime shown in Fig. 6. Details can be found in [10].

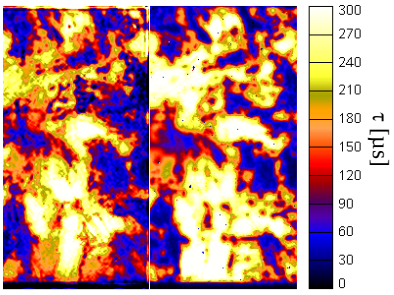

Figure 6: CDI lifetime measurement from Fig. 4, left, corrected by deconvolution (left). For comparison, the reference measurement with chemically polished surface is shown on the right.

3 QUANTITATIVE PHOTOLUMINESCENCE IMAGING

Photoluminescence Imaging (PLI) is a fast technique for lifetime measurements [6]. We have now developed a calibration procedure which accounts for reabsorption, thickness variation and doping concentration. The PLI signal depends on the Δn(z)-profile:

$$I_{PL} = K_{cal} \int_{\lambda_{min}}^{\lambda_{max}} \eta_{camera}(\lambda) T_{filter}(\lambda) dj_0(\lambda) \times \int_{z=0}^{d} \left(\Delta n^2(z) + \Delta n(z) N_A\right) \exp(-\alpha(\lambda) z) dz d\lambda \,, \quad (3)$$

where K_{cal} is a calibration factor, η_{camera} is the quantum efficiency of the camera, T_{filter} is the transmission of the long-pass filters used for suppression of reflected laser light, j_0 is the band-to-band luminescence spectrum without reabsorption effects, N_A is the base doping concentration and α is the absorption coefficient. Δn(z) has been modeled for various lifetime values in dependence of the wafer thickness and surface recombination velocity using PC1D [11]. The calibration factor K_{cal} accounts for geometrical settings and has to be determined by comparison of the PLI signal and a lifetime image measured by CDI, for example. In Fig. 7 the PLI signal for each pixel is plotted versus a CDI lifetime measurement for adjacent wafers of different thickness.

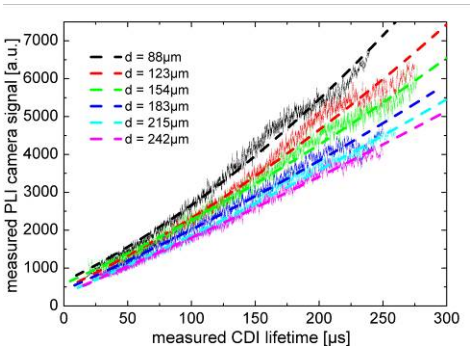

Figure 7: Photoluminescence Imaging versus Carrier Density Imaging. The fit functions (dashed curves) have been obtained from equation (3) including modeled Δn(z)-profiles.

Accounting for the thickness, the expected PLI signal has been calculated and K_{cal} has been used as a fit parameter. It has turned out that K_{cal} is indeed independent from wafer thickness in good approximation. An independent measurement of a different sample with significant larger thickness yields very comparable results to a respective CDI measurement (see Fig. 8) if the calibration factor from Fig. 7 is used.

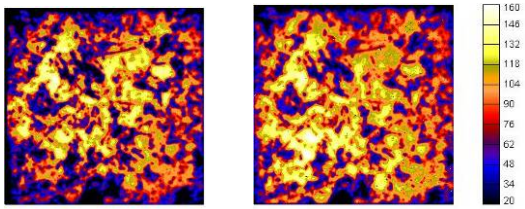

Figure 8: Calibrated PLI measurement (left) and reference measurement with CDI (right). Lifetimes in µs.

Further details can be found in [12] where in addition to this calibration a spatially resolved self consistent calibration approach is alternatively suggested.

4 DIFFUSION LENGTH IMAGING

The spatially resolved diffusion length can be obtained by the Spectrally Resolved Light Induced Current (SR-LBIC) [13] technique. In a recent publication [14] Photoluminescence Imaging measurements with different filters have been used to determine the diffusion length. We now present a different approach which relies on an analytical

description of the infrared signal. Both, CDI and PLI are in principal suitable for diffusion length measurements. We show in the following an approach with CDI on cells with dielectric highly reflective rear side and give a comment on the application of this idea to PLI meausurements.

4.1 Diffusion length measurements on cells with CDI

CDI measures free carrier infrared absorption and emission. In the case of emission CDI on wafers the sample under test is placed on a thermostated mirror which is in thermal equilibrium with the sample. Due to the small emissivity of the mirror, it emits photons at very low flux densities and rather reflects photons from the surroundings. The photon flux density coming from the mirror is therefore strongly dependent on the surrounding room temperature. Depending on the local free carrier density in the wafer in the cell, these photons are partly absorbed by free carrier absorption before being detected by the camera. Additionally, photons emitted by free carriers from inside the sample bulk are detected. Multiple reflections at the wafer surfaces may occur due to small reabsorption effects which enlarge the optical path. A CDI measurement essentially consists of the difference between the detected photon flux density under illumination, i.e. with an increased amount of excess carriers, and under dark conditions. Free carrier emission results in a positive signal whereas the absorption process is detected as a negative contribution which decreases the measurement result. If sample temperature and room temperature are equal, absorption and emission are also equal and no signal is detected. In the extreme case that the temperature of the sample is lower than room temperature an effective (negative) absorption signal is detected. In Fig. 9 a simulation of the CDI signal in dependence of the mirror emissivity for various sample temperatures is shown. Multiple reflections are considered in the simulation.

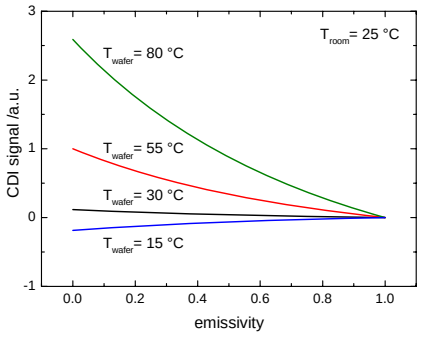

Figure 9: Simulation of CDI signal as function of mirror emissivity.

In order to increase the signal it is therefore important to measure at increased sample temperatures. If the sample is placed on a surface with higher emissivity instead on the mirror the signal decreases significantly. For this reason, CDI measurements on standard industrial solar cells do not yield meaningful results due to the rough aluminum-silicon interface on the back side. CDI has thus been restricted to wafers up to now.

It is nevertheless possible to take advantage of the dielectric and highly reflective rear side of advanced high efficiency solar cell concepts, e.g. laser fired back contacts (LFC). The rear side acts as the mirror of the CDI chuck and emission CDI measurements can be performed. From the measured integral free carrier density the diffusion length can be calculated under some assumptions. Under short circuit conditions, for example, the boundary condition of the base-emitter interface can be described by a vanishing excess carrier density $\Delta n(0) = 0$. Neglecting the contribution of free excess carriers in the space charge region and in the emitter to the CDI signal, the $\Delta n(z)$-profile can be modeled from the continuity equation. An assumption about the surface recombination velocity on the back side S_b has to be made in this model. Equating the integral of $\Delta n(z)$ with the CDI result, the bulk lifetime τ_{bulk} can be calculated. With a given diffusion constant D the diffusion length L_{eff} can be calculated:

$$L_{eff} = \sqrt{D\,\tau_{bulk}}\,. \qquad (4)$$

Fig. 10, left side, shows a diffusion length image calculated from a CDI measurement on a multicrystalline solar cell with LFC rear side and an emitter sheet resistance of 120 Ω/□. On the untextured front side an antireflection coating is deposited. The size of the cell is 100 x 100 mm². On the right side a diffusion length map with the SR-LBIC technique is shown for comparison. The measurement time of the CDI diffusion length image has been 12 min but can even be performed significantly faster. The measurement time for the SR-LBIC map has been two hours.

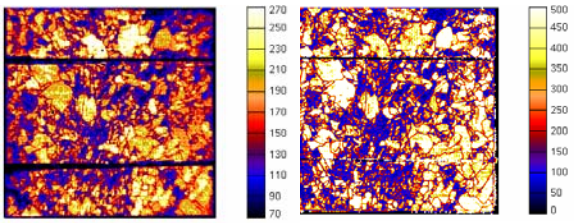

Figure 10: L_{bulk} measurement modeled from CDI measurement (left) and L_{eff} measurement by SR-LBIC (right).

Good qualitative correlation is observed. The absolute value of the left image is too small compared to the SR-LBIC measurement. The width of the L_{bulk}-distribution measured with CDI measurement is smaller which can be observed in Fig. 11. The reason for this observation is still unclear at present.

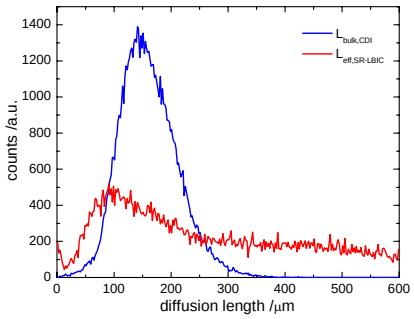

Figure 11: Histograms of measurements shown in Fig. 10.

4.2 Diffusion length measurements on cells with PLI

The modeling of the diffusion length from PLI measurements can in principle be performed along similar lines. An advantage of PLI is that also cells with rough or low reflective rear sides may be measured. Instead of a linear correlation between camera signal and integrated free carrier density, non-linear effects have to be taken into account. These are described in equation (3). Nevertheless, we observed with our setup a significantly lower sensitivity compared to CDI. This is probably due to the smaller laser wavelength of 804 nm used for illumination. The resulting carrier profile is stronger influenced by the front boundary condition due to shallower generation of carriers. The longer wavelength of 940 nm used for the CDI measurements presented above cannot easily be separated from the PL signal by filters due to the small wavelength difference.

5 IMAGING OF TRAP DENSITY

Additionally to the recombination lifetime on wafers and the diffusion length on cells with dielectric reflective rear side, the trap density can be measured with CDI/ILM [4,5]. Measurements under low injection conditions allow the modeling of the Hornbeck and Haynes model to the data and the extraction of the total trap density. It is advantageous that no surface treatment for the wafer is necessary which is in contrast to most of the available lifetime techniques. The total trap density has been found to be closely related to crystal defect density [5] and, for a variety of materials, to the diffusion length of solar cells [15]. This correlation, however, depends on the material, i.e. the crystal quality and/or the impurity content. It has been found, for example, that in cast multicrystalline material the correlation of the trap density distribution in the as-cut wafer and the diffusion length in the corresponding solar cell is high at the bottom of an ingot. However, at the top an anti-correlation has been observed in some regions instead [16]. Trap density and diffusion length measured on a vertically cut wafer and a solar cell made from the same wafer is compared for different heights in the ingot in Fig. 12.

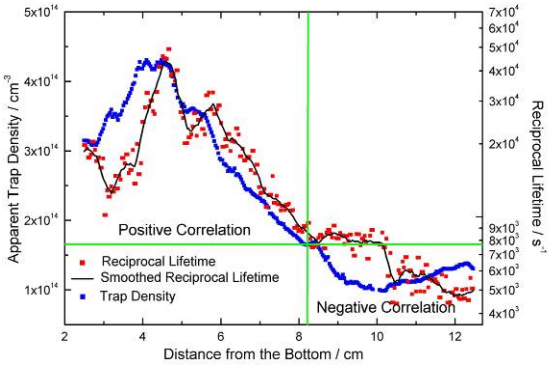

Figure 12: Trap density and reciprocal lifetime as function of vertical position in the ingot for a vertically cut sample.

It is observed that in regions of high trapping, i.e. the bottom part of the ingot in this case, the reciprocal lifetime correlates well with the trap density. At regions with low trapping, i.e. about 8.5 cm above the bottom in our case, an anticorrelation is detected. A possible explanation for the decreasing trap density with height is that the trap centers could be related to oxygen. An increasing influence of impurity metals might be responsible for the negative correlation. Details may be found in [16].

6 CONCLUSION

Infrared imaging methods allow for the detection of a variety of material parameters. Surface conditions have to be correctly taken into account for quantitative measurements. For this purpose a correction method based on emissivity detection and a deconvolution procedure has been presented for Carrier Density Imaging. Progress in quantitative Photoluminescence Imaging has been reported where we are able to calibrate the camera data considering the non-linearity of the PL signal as well as reabsorption effects. CDI on solar cells with dielectric and highly reflective rear side has been shown to give good qualitative information on the diffusion length. Advances in trap density detection with CDI have been reported. A high correlation of recombination in the solar cell and trap density measured in the as-cut material has been observed in the bottom part whereas partial anticorrelation has been detected at increased height in a multicrystalline ingot.

7 ACKNOWLEDGEMENTS

We thank D. Schwaderer, H. Lautenschlager, T. Leimenstoll, F. Heinz, and M. Hermle for sample processing, measurements and fruitful discussions. This work was partly supported by the German Federal Ministry of Education and Research (BMBF) within the framework of the ”Netz Diagnostik” project under contract number 01SF0401.

7 REFERENCES

[1] M. Bail, J. Kentsch, R. Brendel, M. Schulz, Proc. 28th IEEE-PVSC, Anchorage, 99 (2000)
[2] S. Riepe, J. Isenberg, C. Ballif, S.W. Glunz, W. Warta, Proc. 17th EC-PVSC, Munich, 1597 (2001)
[3] J. Isenberg, D. Biro, W. Warta, Prog. in Photov. **12**, 539 (2004)
[4] P. Pohl, J. Schmidt, K. Bothe, R. Brendel, Appl. Phys. Lett. **87**, 142104 (2005)
[5] M.C. Schubert, S. Riepe, S. Bermejo, W. Warta, J. Appl. Phys. **99**, 114908 (2006)
[6] T. Trupke, R. Bardos, M.C. Schubert, W. Warta, Appl. Phys. Lett. **89**, 044107 (2006)
[7] J.A. Hornbeck, J.R. Haynes, Phys. Rev. **97**, 311 (1955)
[8] P.J. Cousins, D.H. Neuhaus, J.E. Cotter, J. Appl. Phys. **95** (4), 1854 (2004)
[9] T. Trupke, R.A. Bardos, M.D.Abbott, Appl. Phys. Lett., **87**, 184 (2005)
[10] M.C. Schubert, S. Pingel, M. The, W. Warta, J. Appl. Phys. **101**, 124907 (2007)
[11] D.A. Clugston, P.A. Basore, Proc. 26th IEEE-PVSC, Anaheim, 207 (1997)
[12] M. The, M.C. Schubert, W. Warta, this conference
[13] W. Warta, J. Sutter, R. Schindler, B.F. Wagner, 2nd PVSEC, Vienna, Austria 1650, (1998)
[14] P. Würfel, T. Trupke, T. Puzzer, E. Schäffer, W. Warta, and S. Glunz, J.Appl.Phys. **101**, 123110 (2007)
[15] M.C. Schubert, W. Warta, Prog. in Photov. **15**, 331 (2007)
[16] P. Gundel, M.C. Schubert, W. Warta, this conference